Sideward Peak of Intermediate Mass Fragments in High Energy Proton Induced Reactions *

Yuichi Hirata [a,d,f], Akira Ohnishi [a], Yasushi Nara [b],
Toshihiko Kido [d,h], Toshiki Maruyama [d], Naohiko Otuka [a,g],
Koji Niita [c], Hiroshi Takada [e], Satoshi Chiba [d]

[a] *Division of Physics, Graduate School of Science,*
Hokkaido University, Sapporo 060-0810, Japan

[b] *RIKEN BNL Research Center,*
Brookhaven National Laboratory, Upton, NY 11973, USA

[c] *Research Organization for Information Science & Technology,*
Ibaraki 319-1195, Japan

[d] *Advanced Science Research Center,*
Japan Atomic Energy Research Institute, Ibaraki 319-1195, Japan

[e] *Center for Neutron Science,*
Japan Atomic Energy Research Institute, Ibaraki 319-1195, Japan

[f] *Human Genome Center, Institute of Medical Science,*
University of Tokyo, Tokyo 108-8639, Japan

[g] *Meme Media Laboratory, Graduate School of Engineering,*
Hokkaido University, Sapporo 060-8628, Japan

[h] *Hitechs Inc., Kurobe 938-0044, Japan*

Abstract

Intermediate mass fragment (IMF) formation in the 12 GeV proton induced reaction on Au target is analyzed by using a combined framework of a transport model (JAM/MF) and a newly developed non-equilibrium percolation (NEP) model. In this model, we can well reproduce the mass distribution of fragments. In addition, the sideward peaked angular distribution would emerge under the condition that the fragment formation time is very short, around 20 fm/c. Within this short time period, the un-heated part of the residual nucleus is kept to have doughnut shape, then the Coulomb repulsion from this shape strengthens the sideward peak of IMF.

Key words: intermediate mass fragment, sideward angular distribution, multifragmentation, Coulomb force
PACS: 25.40.-h, 25.70.Mn, 24.60.-k

1 Introduction

Multifragment formation from excited nuclei has attracted attention in this decade. It is closely related to the properties of nuclear matter, especially to its liquid-gas phase transition. For example, it has been proposed that multifragmentation would be caused by the volume instability of nuclear matter in the spinodal region [1,2], in which nuclear liquid and gas phase rapidly coexist. Although recent high-quality heavy-ion experiments enable us to study the first-order nature of the nuclear liquid-gas phase transition [3–5], whether the origin of multifragmentation is statistical or dynamical is still under debate [6,7]. It is a big challenge for theorists to elucidate the relation between the fragment formation and the equilibrium properties of nuclear matter, including its phase transitions. Therefore, various methods have been proposed in order to extract the signals of critical behavior of nuclear matter in heavy-ion collisions where the system size is finite [8]. In heavy-ion collisions, however, non-trivial roles of strong collective flow make it difficult to relate fragment formations and the nuclear matter properties directly. Thus it is also necessary to investigate fragment formation phenomena in light-ion induced reactions, in which the flow effects on the fragmentation are expected to be smaller.

It has been known that the fragment mass distribution in high-energy proton induced reactions follows the power law, which signals the statistical formation of fragments in a critical but equilibrium condition. Energy spectra of IMFs also support the statistical fragment formation picture. In a recent KEK experiment of 12 GeV proton induced reaction on Au target, the energy spectra of IMFs such as O, F, Ne, and Na are measured, and it is found to be well fitted with a thermal model with Coulomb barrier [9,10]. On the other hand, Pb beam at 1 A GeV in GSI offers a unique possibility to measure fragment production cross sections in inverse kinematics using proton targets [11], and the global structure of isotope mass distributions are also well fitted by an intra-nuclear cascade model [12] followed by a de-excitation model [13]. Thus both of the statistical and dynamical models describe the fragment mass distribution well also in high-energy pA reactions.

Contrary to the mass and energy distribution of fragments, the angular distribution of IMFs contradicts to a picture of the statistical fragmentation from an equilibrated system. It is also long known that the angular distribution of Intermediate Mass Fragments (IMFs) becomes sideward peaked at proton incident energies above $E_p = 10$ GeV [9]. In the above KEK experiments, the angular distribution of IMFs such as O, F, Ne, and Na are shown to have a sideward peak around 70 degrees in the laboratory frame. The same experimental conclusion is also obtained in a BNL-AGS experiment. In the

AGS p+Au experiment [14], the laboratory angular distribution of C isotopes becomes to have sideward peak as the incident energy of proton go beyond 10 GeV. This sideward peaked feature has been considered to be a mystery; it contradicts to a naive picture of statistical fragment formation from a spherical equilibrated residual nuclei.

In a statistical picture of fragment formation, the angular distribution of fragments is generally forward peaked. At low energies, the incident proton is absorbed into the target, and forms a thermalized compound nucleus having the incident proton momentum. At high energies, the incident proton collides with nucleons inside target nucleus (cascade process) in the first stage of reactions. These successive two-body scatterings give momentum transfers to the nucleons in target, and some of them are emitted from the residual nucleus. The momentum transfer to the residual nucleus is in the forward direction in average. Thus in both cases, the residual excited nucleus should have a forward momentum in average. If this residual compound nucleus decays statistically, produced fragments should have forward peaked angular distribution.

It is expected that these fragment angular distribution anomaly would be due to a new fragment formation mechanism, which becomes evident at higher incident energies. This new mechanism would be related to a new property of excited nuclei produced in GeV proton induced reactions. For the understanding of this sideward emission of IMFs, several characteristic mechanisms have been proposed so far; the shock wave propagation [15], the strange shaped nucleus formation [16,17] which is also predicted to be formed in heavy ion collisions [18], and recoil effects of particle scatterings [14]. However, there is neither decisive conclusion nor satisfactory explanation for the sideward peak of IMF angular distribution, since it is not an easy task to analyze this phenomenon theoretically.

In the first stage of the high-energy proton induced reaction, the incident proton interacts with target nucleons and produces several pions. In the incident energy range around 10 GeV, the reaction mechanism of hadron-hadron collision evolves from single resonance baryon production to mutual excitation of incident baryons and/or string formation. For a reliable description of high-energy pA reactions, it is necessary to invoke these incident-energy dependent elementary cross sections parametrized and verified in pp and pA reactions. In Ref. [19], a hadron-string cascade model (JAM) is developed, and it is successfully applied to hh and pA reactions as well as AA reactions. In the next stage of the reaction, scattered nucleons evolve in the mean field and then form an excited residual nuclei. Since the nucleon kinetic energy ranges from a few MeV to around 10 GeV and the fragment mass ranges from two (deuteron) to around 200, it is necessary to invoke appropriate mean field which takes account of the energy dependence as well as the density dependence and is verified in pA reactions. Within a framework of the Quantum Molecular Dy-

3

namics (QMD) [20] which was developed in order to describe fragmentation, a parameterization of nuclear mean field is proposed in Ref. [21], and this mean field is verified in pA reactions in a wide range. In addition, it is already shown to well describe the incident energy dependence of the nucleon potential depth and the binding energy behavior from light to the heaviest nuclei. This mean field has been extended and successfully applied to study nuclear matter properties at sub-saturation densities in later works [22,23]. In the third stage of the reaction, the residual nucleus breaks up into fragments having various masses including IMFs, and the fragmentation mechanism is not understood well in the case we cannot assume that the system decays statistically from an equilibrated system. In heavy-ion reactions, there are some dynamical transport models which do not assume equilibrium [20,24–26] and well reproduce the IMF multiplicities. In this case, the system expands to sub-saturation density due to the rapid collective expansion from the initial hot and compressed nuclei. At sub-saturation densities, local density fluctuation is energetically favored, then fragments are easily formed in the dynamical stage. However, in the case of pA reactions, the flow effect is not large and the expansion is not enough to put the system into sub-saturation densities. At around the saturation density, density fluctuation is not energetically favored, but smoothed out during the evolution in a usual mean field type dynamics even if it is generated in the first stage of the reaction. Thus at present, there is no satisfactory microscopic model to describe the non-equilibrium fragmentation process in high energy proton induced reactions.

In order to develop a model of non-equilibrium fragmentation in proton-induced reactions, we start from an equilibrium fragmentation model, percolation. It has been shown that the percolation model gives a good description of mass and momentum distribution of fragments in high-energy proton induced reactions, if we ignore the anisotropy of fragment emission in the residual nuclear rest frame. Since the initial nucleons are assumed to be distributed uniformly in a sphere in the equilibrium percolation model, the fragment angular distribution becomes automatically isotropic in the residual nuclear rest frame. Therefore, it is expected that the fragment angular distribution would be anisotropic if the initial nucleon distribution contains dynamical information of the earlier stage. We here formulate a new Non-Equilibrium Percolation (NEP) model which takes account of initial density and momentum fluctuation generated in the earlier dynamics. In NEP, the nucleon phase space variables are taken from the results of the transport model calculation as the initial condition of percolation, instead of putting nucleons on sites. The bond breaking or connection probability is calculated by using the distance and momentum difference between the two nucleons under consideration, instead of giving a common bond breaking probability for the bonds connecting nearest neighbor sites. By doing these modifications, we can take into account the position and momentum fluctuations of nucleons inside fragment source and study the effects of non-equilibrium features of residual nucleus to the IMF formation

4

processes.

In this paper, we study the sideward enhanced IMF formation mechanism by using a combined framework of a transport model and a newly developed Non-Equilibrium Percolation model. In the transport part, we use the cross sections and particle production algorithm developed in JAM [19], and the mean field verified in QMD [21]. Hereafter we call this transport model, JAM/MF (JAM with mean field). The nucleon phase space information given in the transport model is used as the initial condition of NEP. We find that we can well reproduce the mass and energy distributions of IMFs in a unified way by using the above combined framework. In addition, if we assume that fragments are produced within a short time scale, we can also describe the sideward enhancement of IMF emission.

We find the following reaction mechanism to enhance sideward emission of IMF: In the short time scale (around 20 fm/c), the dynamical effect in the first hadronic cascade stage still remains. Nucleons along the path of the leading incident proton are heated-up and have large momenta in average. Since IMFs are formed mainly in the cold region, the probability of IMF formation is small around the leading proton path. Then the IMF formation points are distributed non-spherically, predominantly distributed in a doughnut shape. After forming fragments in this doughnut shape, Coulomb repulsion between fragments pushes more strongly in the sideward direction in the rest frame of the residual nuclei.

The outline of this paper is as follows. In Sec. 2, we explain the transport model JAM/MF used in this work. In Sec. 3, a newly developed Non-Equilibrium Percolation (NEP) model is explained, and we discuss the validity of this model to show the good reproduction of fragment mass distribution. Next in Sec. 4, we discuss the mechanism of sideward enhancement of IMF emission through the analysis of the production position distribution of IMF, the IMF energy distribution and the IMF angular distribution. Finally in Sec. 5, we summarize this paper.

2   Transport Model for High Energy Proton Induced Reactions

In high-energy ($E_p \gtrsim 10$GeV) proton induced reactions, there are mainly three stages — hadronic cascade, mean field evolution, and fragmentation. During these stages, nucleon energy decreases by about four order of magnitude from around 10 GeV to a few MeV. A large part of the proton incident energy (~ 10 GeV) is carried away by produced pions and emitted high momentum nucleons, and only a part of this energy remains as the excitation energy of the residual nucleus (several hundred MeV to a few GeV). This

residual nuclear excitation energy is mainly exhausted to breakup the residual nucleus into fragments and nucleons, then the energy of finally produced fragments are around a few MeV per nucleon.

For a reliable microscopic description of dynamical evolution of the system throughout these stages, it is necessary to apply reliable hadronic cross sections for hadronic cascade processes, and well verified mean field. In this work, we have developed a transport model, JAM/MF, by extending the hadron-string cascade model JAM [19] to include the mean field developed in Ref. [21]. It can be also considered as a version of QMD with hadronic cross sections developed in JAM. The results of JAM/MF are used as the initial configuration of the Non-Equilibrium Percolation described in the next section.

2.1 Hadronic cascade processes in JAM

Here we describe the outline of the hadron-string cascade model, JAM. The detail of JAM is described in Ref. [19]. The main components of JAM are as follows.

(1) Nuclear collision is assumed to be described by the sum of independent binary hh collisions. Each hh collision is realized by the closest distance approach. In the original version of JAM, no mean field effect is included, therefore the trajectory of each hadron is straight in between two-body collisions, decays or absorptions.

(2) The initial position of each nucleon is sampled by the parameterized distribution of nuclear density. Fermi motion of nucleons are assigned according to the local Fermi momentum.

(3) All established hadronic states, including resonances with masses up to around 2 GeV, are explicitly included with explicit isospin states as well as their anti-particles. All of them can propagate in space-time.

(4) The inelastic hh collisions produce resonances at low energies while at high energies ($\sqrt{s} \gtrsim 4$GeV in BB collisions $\sqrt{s} \gtrsim 3$GeV in MB collisions and $\sqrt{s} \gtrsim 2$GeV in MM collisions) color strings are formed and they decay into hadrons according to the Lund string model [27]. In JAM, minimum string mass is set to be 2 GeV, which is the same as the default value in the original Lund string model [27]. Therefore, there is no difficulty to use the string model in pA reactions at around 10 GeV, and it has been already shown that we can fit the pp data well [19]. Other string models like RQMD [28] and UrQMD [29] also work very well in the same energy region. Formation time is assigned to hadrons from string fragmentation. Formation point and time are determined by assuming yo-yo formation point. This choice gives the formation time of roughly 1 fm/c with string tension $\kappa = 1$GeV/fm.

(5) Hadrons which have original constituent quarks can scatter with other hadrons assuming the additive quark cross section within a formation time. The importance of this quark(diquark)-hadron interaction for the description of baryon stopping at CERN/SPS energies was reported by Frankfurt group [28,29].

(6) At very high energies ($\sqrt{s} \gtrsim 10\text{GeV}$), multiple minijet production is also included in the same way as the HIJING model [30] in which jet cross section and the number of jet are calculated using an eikonal formalism for perturbative QCD (pQCD). Hard parton-parton scatterings with initial and final state radiation are simulated using PYTHIA [27] program.

(7) Pauli-blocking for the final nucleons in two-body collisions are also considered.

(8) We do not include any medium effect such as string fusion to rope [31,28], medium modified cross sections and in-medium mass shift. All results which will be presented in this paper are those obtained from the free cross sections and free masses as inputs.

Hadron (proton, π^+, π^-, K^+, K^-) transverse mass m_t in proton induced reactions ($p(14.6\text{GeV/c})$ + Be, Al, Cu, Au), light-heavy ion induced reactions (Si(14.6 A GeV/c)+ Al, Cu, Au), and heavy-ion reactions (Au(11.6 A GeV/c) + Au) has been analyzed in JAM, and it is found that JAM results show good agreement with the experimental data without any change of model parameters [19]. This means that momentum distributions of isolated single proton are correctly calculated by collision cross sections of JAM.

On the other hand, it is required to take account of later mean field evolution and percolation processes for the description of IMF production.

2.2 Propagation in Quantum Molecular Dynamics

In the framework of Quantum Molecular Dynamics (QMD), the classical trajectory of hadrons is determined by the stochastic hadronic collisions, described in the previous subsection, and the Newtonian equation of motion. The single particle wave function of each nucleon is represented by a Gaussian wave packet, having the phase space centroid parameter of $(\mathbf{R}_i, \mathbf{P}_i)$ for the i-th nucleon. The total wave function is assumed to be a product wave function of nucleon Gaussian wave packets. Then we can derive the Newtonian equations of motion on the basis of the time dependent variational principle [20]. The equations of motion become the canonical equations of the Gaussian centroid parameters as phase space variables,

$$\dot{\mathbf{R}}_k = \frac{\partial H}{\partial \mathbf{P}_k} , \quad \dot{\mathbf{P}}_k = -\frac{\partial H}{\partial \mathbf{R}_k} . \tag{1}$$

The Hamiltonian H consists of the kinetic energy and the effective interaction energy.

$$H = T + V \ , \tag{2}$$

$$T = \sum_i E_i = \sum_i \sqrt{m_i^2 + \mathbf{P}_i^2} \ , \tag{3}$$

$$V = V_{\mathrm{Skyrme}} + V_{\mathrm{Sym}} + V_{\mathrm{Mom}} + V_{\mathrm{Coul}} + V_{\mathrm{Pauli}} \ . \tag{4}$$

In this interaction energy, the following terms are included: Skyrme type density dependent interaction (V_{Skyrme}), symmetry energy (V_{Sym}), momentum dependent interaction taking account of the energy dependence of the nucleon potential (V_{Mom}), Coulomb potential between protons (V_{Coulomb}), and the Pauli potential (V_{Pauli}). The last term is added to take into account the Pauli principle approximately. The form of each term is shown in the Appendix.

In this study we use parameters shown in Table A.1. These parameters are determined to reproduce various kinds of systematic observables such as (1) the density dependence of the total kinetic energy of Fermi gas, (2) density dependence of the total energy of symmetric nuclear matter above normal nuclear density, and (3) energy dependence of the real part of proton-nucleus optical potential, binding energy and radius of heavy nuclei ($A > 3$). All these observables are calculated by Metropolis sampling method under the condition that the temperature of nucleus is 2.5 MeV. Including the Pauli potential improves the description of the quasi-elastic part of the neutron energy spectra in p(256MeV,800MeV)+^{208}Pb [21]. The same form of the interaction and an improved version by including the surface term have been applied to study nuclear matter properties at sub-saturation densities [22,23] in addition to the above points (1)-(3).

In the simulation of 12 GeV proton induced reaction, the ground state of target nucleus (Au) is calculated by frictional cooling and heating method to fit the binding energy of Au.

In the total Hamiltonian H we have already introduced the relativistic form of kinetic energy expression and adopted the relativistic kinematics in the cascade processes in JAM. In order to make a full relativistic description, it is also necessary to formulate the interaction terms in a covariant way. A Lorentz-covariant extension of the QMD, dubbed relativistic quantum molecular dynamics (RQMD), has been proposed in Ref. [32], which is based on the Poincaré-invariant constrained Hamiltonian dynamics. Although the RQMD is a numerically feasible extension of QMD towards a fully covariant approach, it still costs too much computing time to apply to heavy systems. Therefore, we make an alternative extension of QMD [33]. We introduce Lorentz-scalar quantities into the arguments of the interactions,

$$\mathbf{D}_{ij}^2 = (\mathbf{R}_i - \mathbf{R}_j)^2 \rightarrow \tilde{\mathbf{D}}_{ij}^2 \equiv -D_{ij}^2 + (P_{ij} \cdot D_{ij})^2/P_{ij}^2 \ , \tag{5}$$

$$\mathbf{Q}_{ij}^2 = (\mathbf{P}_i - \mathbf{P}_j)^2 \rightarrow \tilde{\mathbf{Q}}_{ij}^2 \equiv -Q_{ij}^2 + (P_{ij} \cdot Q_{ij})^2/P_{ij}^2 \ . \tag{6}$$

In these expressions, thin letters (D_{ij}, Q_{ij}, P_{ij}) show four vectors, and P_{ij} denotes the two-body center-of-mass four momentum

$$P_{ij} \equiv P_i + P_j = (E_i + E_j, \mathbf{P}_i + \mathbf{P}_j) \ . \tag{7}$$

It is easy to show that the quantity $\tilde{\mathbf{D}}_{ij}^2$ is the two-body distance squared in the two-body CM system. By these procedures we can take into account the primary part of the relativistic dynamical effects approximately in our QMD.

3 Fragment Formation

There are many attempts to describe the IMF formation in multifragmentation processes by using microscopic molecular dynamics (MD) simulations. Since nuclear fragmentation is a truly quantum-mechanical process and it is beyond the applicability limit of semi-classical MD theory, it is necessary to improve MD theory to include quantum mechanical effects [25,26,34–37]. In Ref. [34,37], the widths of nucleon wave packets are treated as time-dependent dynamical variables. With this extension, we can find significant improvements in ground state properties such as binding energies, density profiles or α-clustering structure in light nuclei, nucleon emission or disintegration of clusters in medium energy heavy-ion collisions. Another type of proposed modification is to include quantum fluctuation or quantum branching [25,26,35]. In Refs. [25,35], the authors discussed the necessity of quantum fluctuation in the equation of motion of MD in order to ensure that the wave packet distribution follows the quantum statistics at equilibrium. The effects of quantum fluctuation in fragmentation processes such as evaporation of particle and fission like fragmentation are discussed in Ref. [35]. The necessity of quantum branching is discussed in Refs. [26,36]. The authors introduce the quantum branching process to compensate the restriction on the one body nucleon distribution, and incorporate the diffusion and the deformation of wave packets according to the Vlasov equation [26]. By this modification, the nucleon motion in the mean field is improved, and the fragment mass distribution is successfully reproduced in heavy ion reactions.

It may be possible to improve the description of IMF formation also in high-energy pA reactions by making above modifications. However, all of these modifications are formulated in non-relativistic ways, and the way to include quantum effects is under discussion. Thus in this work, we treat the fragmentation process in a more phenomenological manner.

In a standard treatment of fragment formation, first we calculate the formation of excited fragments in a transport model or in a phenomenological way, then *provided that these fragments are thermalized* they are forced to de-excite through particle emission and/or fission in a statistical model by using only a few quantities of fragments such as the mass, excitation energy and angular momentum. Since we would like to address the non-equilibrium properties of fragment formation in high-energy pA reactions, here we do not assume that nucleons are distributed uniformly but utilize information in the dynamical stage — nucleon spatial and momentum distribution inside the residual nuclei generated in the transport model, JAM/MF. In order to activate these nucleon phase space degrees of freedom in fragmentation processes, the percolation model would be an appropriate starting point. In percolation models, nucleon positions are already considered, and we can easily assign the momentum to each nucleon.

In this section, we explain our prescription to form residual nuclei from transport model results, and how to incorporate non-equilibrium nature in the percolation model.

3.1 Residual nucleus formation

After successive collisions and mean field evolution of nucleons, several particles are emitted and a residual nucleus is formed. Here, we take all phase space information of all particles consisting the system. Then we can obtain physical property of residual nucleus such as charge, mass and excitation energy as follows.

We assume an external nuclear mean field of nucleons around the residual nuclei having a depth of 50 MeV. Then we assume that particles are trapped and form a residual nucleus when the nucleon single particle energy is negative (for neutrons) or below the Coulomb barrier (for protons). The excitation energy E^* of the residual nucleus is calculated in a similar way to that in the exciton model [38]. Here, we assume the nucleon Fermi energy in the residual nuclei ε_F is 40 MeV.

$$E^* = \sum_{i=1}^{N_h} \varepsilon_i^h + \sum_{j=1}^{N_p} \varepsilon_j^p \ , \tag{8}$$

$$\varepsilon_i^h = \varepsilon_F - \bar{\varepsilon}_i \ , \quad \varepsilon_j^p = \varepsilon_j - \varepsilon_F \ . \tag{9}$$

Here $\bar{\varepsilon}_i$ denotes the target nucleon single particle energy just before the first collision of that target nucleon, then the hole number (N_h) corresponds to the number of target nucleons which collide with the leading proton or secondary

cascade particles. The particle energy ε_j is the scattered nucleon single particle energy at the time of residual nucleus formation. The number of particles (N_p) is calculated at the residual nucleus formation. This method is basically the same as that of Ref. [39].

3.2 Non-Equilibrium Percolation model

In (bond) percolation models, nucleons in the residual nucleus are put on the lattice sites, and we cut the bond between the nearest neighbor sites according to the bond breaking probability given as a function of excitation energy. Then the connected nucleons are assumed to form fragments. By estimating the excitation energy and the mass of the residual nucleus in a simple physical model, it has been demonstrated that the percolation model works very well to describe the mass and energy distribution of fragments produced from multifragmentation processes in relativistic energy (> 10 GeV) pA reactions [40–42].

In standard percolation models, there is one strong assumption which disables us to describe IMF anisotropy: the total excitation energy is assumed to be uniformly distributed over the entire excited system of the residual nucleus, and the nucleons are spatially distributed uniformly in a sphere. This is equivalent to assume that equilibrium is reached in the residual nucleus. This assumption is very convenient to discuss some formal aspects of the model, such as the critical bond breaking probabilities, critical exponents, and so on. In reality, the nucleon may not be uniformly distributed spatially and the excitation may depend on the position inside the residual nucleus, if the fragmentation time scale is short. Therefore, as a natural extension of the percolation model to include non-equilibrium effects, we start percolation from nucleon phase space distribution given in the dynamical transport model calculation. In this case, since nucleons are not necessarily on the lattice sites, the bond breaking probability becomes a function of distance between the nucleon pair. In addition, we can consider the position dependence of the bond breaking probability.

Here we propose a Non-Equilibrium Percolation (NEP) model without lattice combined with a transport model. We start from nucleon phase space distribution given in the microscopic transport simulation, and the bond breaking probability is parametrized as a function of nucleon pair distance and positions. In the following, we explain the actual calculation procedure in NEP.

(1) Dynamical evolution of the pA reaction is simulated by using the transport model described in the previous section, Sec. 2, until $t = t_{sw}$.
(2) Phase space information of nucleons inside the residual nucleus, and the

11

bulk quantity of the residual nucleus such as charge Z_{res}, mass A_{res} and excitation energy E^* are obtained according to the prescription described in the previous subsection, Subsec. 3.1.

(3) All nucleons inside the residual nucleus are connected by bonds.

(4) Neighbor sites are selected by breaking the bond when the bond length L_b is large enough, and the total excitation energy dependence of the bond breaking is taken care of. When the total excitation energy exceeds a given value, $E^* \geq E_0(A_{res})$ ($E_0 = 8c_1 A_{res}$ MeV), the bond is broken if $L_b > R_{cut}$. When the total excitation energy is small, $E^* < E_0(A_{res})$, bonds are broken if $L_b > c_2 R_{cut}$. This total excitation energy dependence is necessary to keep the residual nucleus stable at low excitation. For example, if we set $c_2 = 1$, we underestimate the fragment yield whose mass is very close to the target nucleus, but it does not affect the IMF yield significantly.

(5) The bond between the i-th and j-th nucleons is broken with a probability $p_b(i, j)$. The bond breaking probability $p_b(i, j)$ depends on the local excitation of the residual nucleus, and it is parametrized as follows.

$$p_b(i, j) = 1 - \exp\left[-\nu E^*(\mathbf{R}_{ij})\right] \tag{10}$$

Here, $E^*(\mathbf{R}_{ij})$ is the local excitation energy at the center-of-mass position ($\mathbf{R}_{ij} = (\mathbf{R}_i + \mathbf{R}_j)/2$) of the nucleon pair. We calculate $E^*(\mathbf{R}_{ij})$ as follows,

$$E^*(\mathbf{R}_{ij}) = \sum_k e_k^* \exp\left[-\frac{(\mathbf{R}_{ij} - \mathbf{R}_k)^2}{a^2}\right] \; , \tag{11}$$

$$e_k^* = \begin{cases} t_k - e & (t_k \geq e) \\ 0 & (t_k < e) \end{cases} \; , \tag{12}$$

where t_k is the kinetic energy of k-th nucleon in the CM frame of the residual nucleus and $\mathbf{R}_k$ is the position of k-th nucleon. In this work, the Fermi kinetic energy e is assumed to be a constant for simplicity, since the density does not drastically change in pA reactions.

(6) Fragments are identified as the bond connected nucleons at this stage. The fragment momentum $\mathbf{P}_f$ and position $\mathbf{R}_f$ are determined as the CM momentum and position of nucleons belonging to this fragment.

The model parameters, $R_{cut}, \nu, a, e, c_1, c_2$, are determined to fit the mass distribution of fragments produced in $p(11.5\text{GeV})+$Au reaction. The values of NEP parameters are shown in Table 1.

Table 1
Parameters of NEP

R_{cut}(fm)	ν(1/MeV)	a(fm)	e(MeV)	c_1	c_2
2.1	600	2.0	45.0	0.2	1.1

In Fig. 1, we show the calculated fragment mass distributions in $p(12$
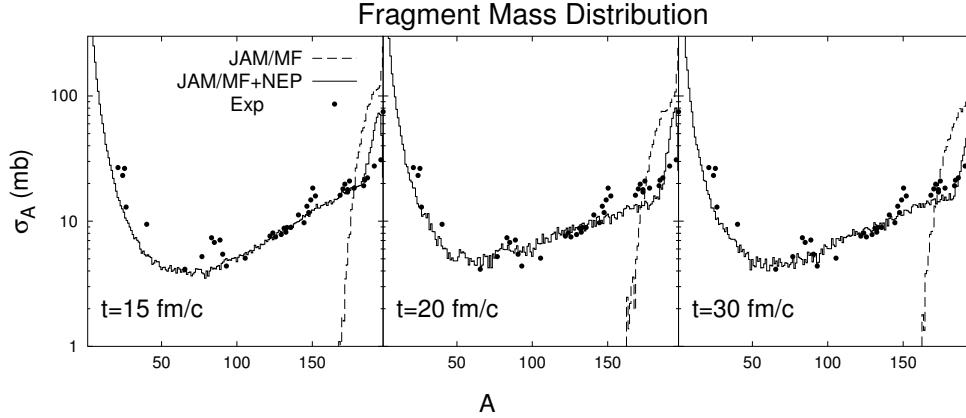
Fig. 1. Calculated fragment mass distributions in $p(12 \text{ GeV})+Au$ reaction. Dashed histograms and solid histograms show calculated results of JAM/MF and JAM/MF followed by NEP, respectively. In the left, middle and right panels, the dependence on the the switching time ($t_{sw} =15$, 20, and 30 fm/c, respectively) is shown. Solid points show the experimental data of $p(11.5\text{GeV})+Au$ reaction [43]. In the transport model, simulation calculations are made in the impact parameter range of $b \leq 7.5$ fm.

GeV)+Au reaction in comparison with the experimental data [43]. The mass of residual nucleus (dashed histograms) is distributed in the range $160 \lesssim A_{res} \lesssim 197$. This means that, in the transport model simulation, the number of emitted nucleons is less than 40. Then, the decay of the residual nucleus to various mass fragments is described in NEP as shown by the solid histograms. (We have checked the stability of the target nuclei in JAM/MF by running the program until $t = 30$ fm/c without shooting a proton into the nucleus and employing the NEP model. We have found that that the average number of evaporated nucleons is around one. Although this evaporation is an artificial effect in our approach, this number is much smaller than that of dynamically emitted nucleons in pA reactions and it would not cause any serious influence on the results shown in this paper.)

One can see that the characteristic U-shape curve of the experimental mass distribution is well reproduced in our calculation, and this behavior does not strongly depends on the switching time. When we analyze the impact parameter dependence of the mass distribution, we find that this U-shape distribution is a consequence of the integration over the impact parameter. In central collisions, the residual nucleus generally has smaller mass and larger excitation energy, and it decays into smaller fragments, in average. In peripheral collisions, the residual nucleus is not highly excited, and emits only several nucleons and very small fragments leaving a heavy nucleus as a remnant in the percolation stage.

This behavior may be more clearly understood in terms of the bond break-

13

ing probability [40]. In standard percolation models, when the bond breaking probability is greater than the critical value, $p_b > p_{crit}$, smaller fragments are favored and the mass distribution shows an exponentially falling behavior. On the other hand, with $p_b < p_{crit}$, large fragments are favored and the mass distribution has a two peak structure (nucleons and heavy nuclei). At around the critical value, $p_b \sim p_{crit}$, the fragment size distribution approximately follows a power law, which creates IMFs effectively. Although the bond breaking probability $p_b(i, j)$ depends on the nucleon pair and events in NEP, the mean value $\overline{p_b}$ (over the pairs and events) behaves as a decreasing function of the impact parameter, from $\overline{p_b} > p_{crit}$ in central collisions to $\overline{p_b} < p_{crit}$ in peripheral collisions. Thus integrating over the impact parameter results in the U-shape mass distribution, whose mechanism is essentially the same as that in the standard percolation models [40].

Because of the above fragment formation mechanism, the global U-shape feature of the mass distribution can be also reproduced in a standard percolation model. In Fig. 2, we show the model dependence of the mass distribution. Here we compare the combination of the models, JAM with Statistical Decay Model (SDM) [33], Percolation model, JAM with Percolation model, and JAM/MF with NEP. In SDM, the evaporation of light fragments $(n, p, d, t, {}^3\mathrm{He}, \alpha)$ and the fission of heavy nuclei are included, but these are not enough to form IMFs abundantly. On the other hand, in the percolation model of Ref. [41] which fit the mass distribution of $p+\mathrm{Ag}$ reaction at 300 GeV, the global mass distribution is reproduced without any change of the model parameters, and it is possible to get a better fit by using target dependent parameters.

This comparison of model calculations suggests the necessity to invoke some kind of multifragmentation mechanism such as the percolation in addition to the evaporation and fission. If we adopt the percolation model in fragmentation stage, we can qualitatively describe the U-shape mass distribution, which we cannot explain in statistical decay models with evaporation and fission. Furthermore, in order to reproduce the whole range of the mass spectrum, it is necessary to stabilize the nucleus at low excitation. In the original percolation model [41] (upper right panel), nucleon positions are kept to be on sites, and the bond breaking probability becomes smaller in peripheral collisions, then larger mass nuclei can survive. With QMD transport (lower right panel), heavy residual nuclei can survive percolation at low excitation, because the mean field keeps the nucleus stable. Without mean field (lower left panel), on the other hand, nucleons with moderate kinetic energy can easily escape from residual nuclei, then we cannot form stable heavy nuclei.

This comparison tells us the merit to use a combined framework of JAM/MF with percolation for the analysis of the fragmentation processes. However, it is possible to reproduce the mass spectra without invoking spatial and/or
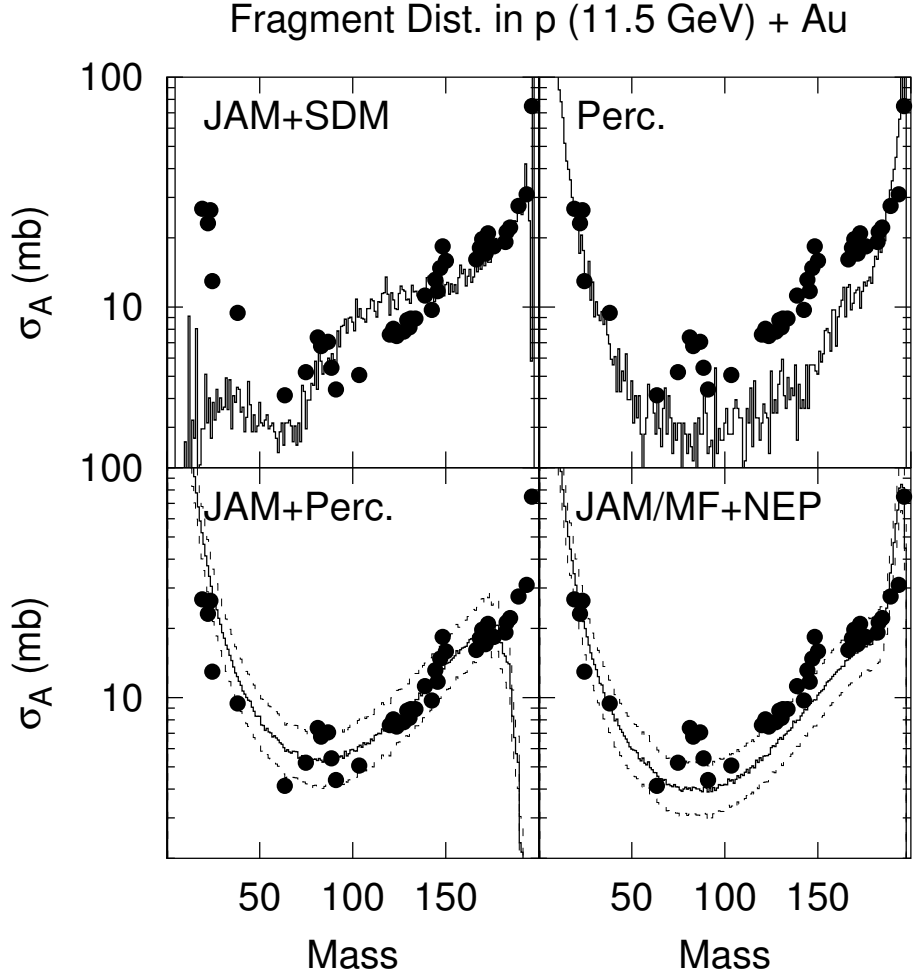
Fig. 2. Model comparison of fragment mass distribution in $p(12 \text{ GeV})+$Au reaction. Four model results — JAM+SDM [33] (upper left), Percolation model with default parameters (upper right) [41], JAM+Percolation (bottom left), JAM/MF + NEP (bottom right) — are shown in histograms and compared with the experimental data [43]. As for the explanation of these models, see the text. Dashed histograms in the lower panels show the calculated results multiplied by 1.3 and 1/1.3, showing that the combined analyses of a transport model with percolation reproduce the data within around 30 % accuracy.

momentum fluctuation generated in the dynamical stage by modifying parameters. Therefore, for the investigation of non-equilibrium nature in the fragmentation, it is necessary to analyze the energy and angular distribution of fragments.

4 Results

4.1 IMF formation points

Now we analyze the non-equilibrium properties of IMF production in the framework explained in the previous sections. In Fig.3, IMF($6 \leq Z \leq 20$) formation position distributions in xy-plain calculated in the transport model calculation followed by NEP are shown. In the transport model simulations, 5000 events are generated, and the results of NEP from these events are overlaid in the figure. In central events ($b \leq 3$ fm, upper panels), we can see that IMFs are produced in the doughnut shaped region. Along the leading proton path, a large part of nucleons collide with the leading proton or secondary cascade particles. Since they have large kinetic energies, they are not judged to belong to the residual nuclei. Even if they stay in the residual nuclei, the local bond breaking probability becomes large. As a result, the IMF formation is suppressed along the leading proton path. In the surrounding doughnut shaped region, the number of collision is small, then the excitation energy is low.

In the lower panels of Fig.3, IMF formation points in peripheral collisions (3 fm $\leq b \leq 7.5$ fm) are shown. We can see that IMFs are produced from a new moon shaped region. In peripheral collisions, highly excited region is shifted to outer side. Then peripheral excited region shrinks to narrower at around the time 30fm/c.

In Fig. 4, we show calculated IMF formation points in xz-plain, restricted to $|y| \leq 2.0$ fm. We can see that IMF formation point distributions clearly have a hole along the leading proton path in central collisions (upper panels) and at early times in peripheral collisions (lower panels).

In both of the cases, IMFs are formed mainly on the surface of the residual nuclei, and the formation is suppressed in the central part. This feature can be understood as follows. When the excitation energy is small, nucleons are likely to be connected with each other. In the central part of the residual nucleus, IMF can grow easily to heavier nucleus by being connected with cold nucleons in the surrounding region. This mechanism may emerge also in the equilibrium percolation model. However, this will not generate any anisotropy in IMF angular distribution.
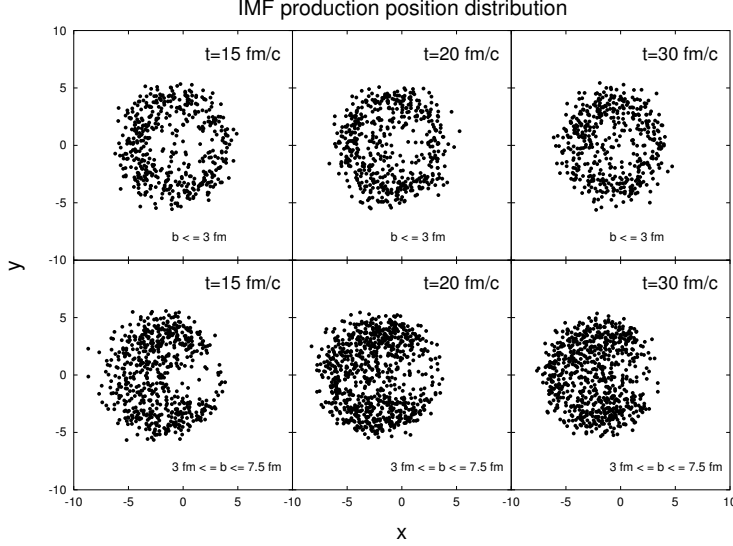
16

Fig. 3. Calculated IMF ($6 \leq Z \leq 20$) position distributions in xy-plain. Solid points display the IMF formation points in NEP following the transport model evolution until the switching time of 15, 20 and 30 fm/c. 5000 events of the transport model events are overlaid. In upper and lower panels, central ($b < 3$ fm) and peripheral ($3 \leq b < 7.5$ fm) events are shown, respectively.

4.2 IMF energy distribution

After the fragments being simultaneously produced through the multifragmentation of the residual nucleus, the fragments are dispersed by the Coulomb repulsion. In the uniform Coulomb expansion of fragments, the total fragment kinetic energy is calculated as the sum of the thermal and the Coulomb energies. In order to describe the Coulomb expansion of fragments, here we consider the following classical Hamiltonian H,

$$H = \sum_{i=1} \sqrt{\mathbf{P}_{fi}^2 + m_{fi}^2} + \sum_{i<j} \frac{Z_{fi}Z_{fj}e^2}{|\mathbf{R}_{fi} - \mathbf{R}_{fj}|} \tag{13}$$

where m_{fi}, $\mathbf{R}_{fi}$, Z_{fi} and $\mathbf{P}_{fi}$ are the mass, position, charge, and momentum of the i-th fragment, respectively. From this Hamiltonian Eq.(13), the Newtonian equations of motion are solved numerically. The initial values of the $\mathbf{R}_{fi}$ and $\mathbf{P}_{fi}$ are given in NEP as discussed in Sec. 3. The time evolution of the Coulomb expansion is solved until the total kinetic energy of each fragment ceases to show appreciable changes. Then we obtain kinetic energies of fragments in the final state. Here, we adopt the time step of Δt=0.5 fm/c and integration until 500 time steps are carried out.

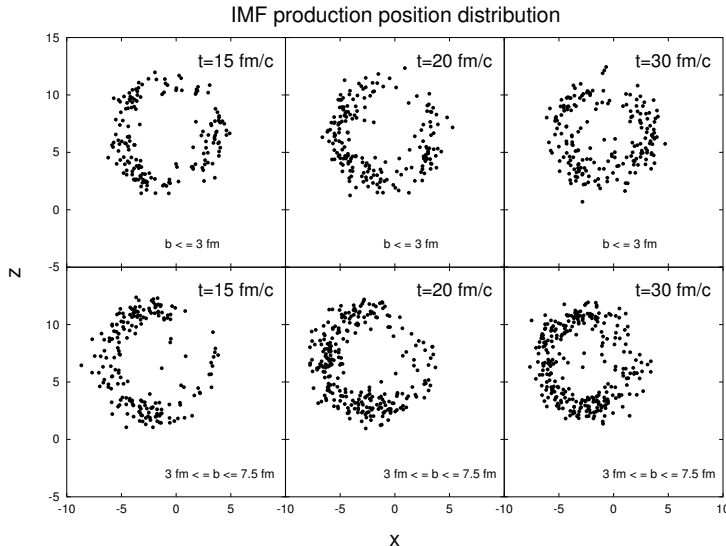In Fig. 5, we compare the calculated IMF energy distributions produced in

17

Fig. 4. Calculated IMF ($6 \le Z \le 20$) position distributions in xz-plain, restricted to $|y| \le 2.0$ fm. Solid points display the IMF formation points in NEP following the transport model evolution until the switching time of 15, 20 and 30 fm/c. 5000 events of the transport model events are overlaid. In upper and lower panels, central ($b < 3$ fm) and peripheral ($3 \le b < 7.5$ fm) events are shown, respectively.

p(12 GeV)+Au reaction with the experimental data [10]. From these results we can see large effects of Coulomb expansion in the energy distribution of IMF. If we take into account only the kinetic energy of fragments calculated in the transport model followed by NEP, the energy peak around 50 MeV is never reproduced. On the other hand, we find that the calculated results after Coulomb expansion reproduce the qualitative behavior of the experimental data well; peaked around 40-60 MeV, enhancement at sideward angles, and the absolute values of the double differential cross sections. These facts show us that the Coulomb expansion process plays a very important role in the fragmentation phenomenon.

4.3 Analysis of IMF angular distribution

In Fig. 6, we show the calculated switching time dependence of the IMF angular distribution. In comparing the results with (left panel) and without (right panel) Coulomb expansion, the Coulomb expansion effects are found to modify the angular distribution largely from forward peaked to sideward peaked.

This mechanism is connected with the IMF formation point in the residual nucleus. As shown at Figs. 3 and 4, IMFs are produced dominantly in a dough-nut shaped region in violent central collisions. Then the fragment density is
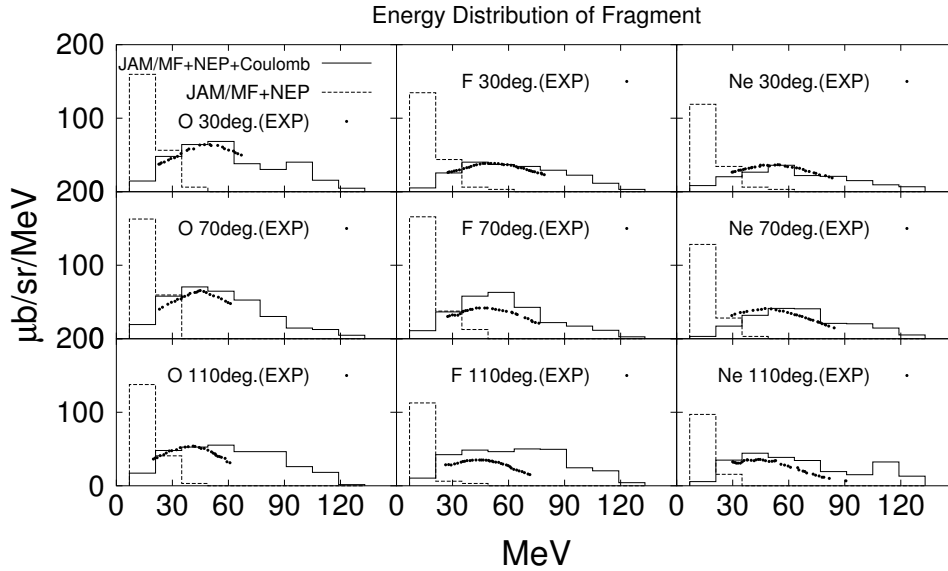
18

Fig. 5. Calculated energy distributions of O, F and Ne isotopes produced in $p(12$ GeV$)$+Au reaction in comparison with the experimental data. The vertical axis shows the cross section and the horizontal axis shows the kinetic energy of the fragment. Left, middle and right panels show the energy distributions of O, F and Ne, respectively. Upper, middle and lower panels show the energy distributions emitted at angles of 30, 70 and 110 degrees from incident proton direction in the laboratory frame. Solid and dashed histograms show the calculated results with and without the Coulomb expansion process. The results of switching time $t_{sw} = 20\,\mathrm{fm}/c$ are shown. Solid points are the experimental data [10]

dense in the doughnut region, and thin in the central region. The Coulomb repulsion between fragments from this configuration pushes IMFs to the sideward direction more strongly than to the forward and backward direction. For example, let us consider the case in which all the fragments are slow and located along a ring, and fast nucleons are distributed uniformly in a sphere. In this case, fast nucleons will escape rapidly, then the Coulomb repulsion acts only in the sideward direction. As a result, the fragment angular distribution would be strongly enhanced at 90° in the rest frame of the ring. Although this is an extreme, the formation point distribution (Fig. 3) and the energy distribution (Fig. 5) of IMFs support this mechanism.

In peripheral collisions, on the other hand, although IMFs are formed in a new moon shaped regions at early times, the anisotropy of the IMF production points is rapidly washed out. Then if the impact parameters are integrated over, the angular distribution of IMFs becomes forward peaked at around the switching time $t_{sw} = 30$ fm$/c$ even after the Coulomb expansion as shown in the left panel of Fig. 6. This observation is consistent with the behavior expected in a equilibrium statistical picture of fragmentation. Therefore, our

19

present study suggests the possibility that IMF angular distribution would have sideward peak at around 90 degrees in the rest frame of the residual nuclei if IMFs can be formed in a very short time scale around 20 fm/c.
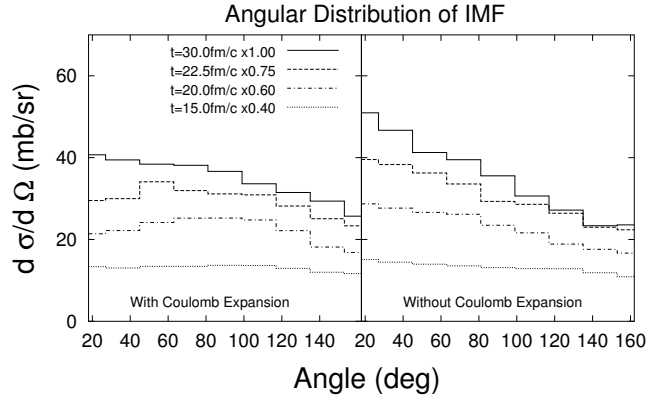

Fig. 6. Calculated switching time dependence of the IMF angular distribution. Dotted, dash-dotted, dashed and solid histograms display the results at switching time of 15, 20, 22.5 and 30 fm/c, multiplied by 0.4, 0.6, 0.75 and 1.0, respectively. In the left (right) panel, the results with (without) Coulomb expansion is shown.

5 Summary

In this paper, we have analyzed the mechanism of formation and sideward enhancement of IMFs produced in the 12 GeV proton induced reaction on Au target by using a combined framework of a transport model (JAM/MF) followed by a newly developed Non-Equilibrated Percolation (NEP) model. NEP can take into account non-uniform spatial distribution of nucleons and the local excitation in the residual nucleus, then it would be appropriate to analyze non-equilibrium natures of IMF formation. The present combined model has been verified in various ways. In the hadronic cascade stage (JAM), momentum distribution of nucleons has been verified by comparing hadron (proton,π^+,π^-,K^+,K^-) transverse mass spectra [19]. The effective interaction in QMD has been verified through the study of matter and nuclear properties and the quasi-elastic neutron energy spectra in pA reactions at 256 MeV and 800 MeV [21]. In the fragmentation (NEP), although there are still several model parameters, they are determined to fit the fragment mass spectra in high-energy pA reactions. By using the same parameter, we applied our model to the fragment energy distributions, and the experimental data are well reproduced.

By using this model we have shown that IMFs are produced in a dough-

nut shaped region and a new moon shaped one inside the residual nucleus in central and peripheral collisions, respectively. We suggest that combined effects of such a geometry of IMF formation point distribution and the Coulomb expansion between fragments would lead to a sideward peaked angular distribution of IMFs provided that the IMFs are formed in a very short time scale of around 20 fm/c. In principle, it would be possible to estimate this time scale experimentally by measuring the particle correlations in momentum multi-dimensions.

One of the remaining interesting problems is to study the mechanism of the incident energy dependence of the IMF angular distribution, which evolves from forward peaked, sideward peaked, to backward peaked as the incident energy grows. Our approach will be also useful in analyzing this problem. Another interesting problem is to elucidate the dynamical aspects of fast fragmentation at around ρ_0 but from a non-spherical shape, which may require other origins of flucutation and correlation than those proposed so far.

Acknowledgements

A   Effective Interaction in Quantum Molecular Dynamics (QMD)

In QMD method, the single particle wave function of the i-th nucleon is represented in a Gaussian wave packet, having the density distribution,

$$\rho_i(\mathbf{r}) = \frac{1}{(2\pi L)^{\frac{3}{2}}} e^{-\frac{(\mathbf{r}-\mathbf{R}_i)^2}{2L}}, \tag{A.1}$$

where L denotes the width parameter for the Gaussian wave packets and $\mathbf{R}_i$ are the centers of position of the i-th nucleon.

Each term in the interaction energy in Eq. (4) depends on the center of

position $\mathbf{R}$ of the nucleon and the center of momentum $\mathbf{P}$ of the nucleon as follows,

$$V_{\text{Pauli}} = \frac{C_{Pauli}}{2(q_0 p_0/\hbar)^3} \sum_{i \neq j} e^{-\frac{(\mathbf{R}_i - \mathbf{R}_j)^2}{2q_0^2} - \frac{(\mathbf{P}_i - \mathbf{P}_j)^2}{2p_0^2}} \delta_{\tau_i \tau_j} \delta_{\sigma_i \sigma_j}, \tag{A.2}$$

$$V_{\text{Skyrme}} = \frac{\alpha}{2\rho_0} \sum_i < \rho_i > + \frac{\beta}{(1+\tau)\rho_0^\tau} \sum_i < \rho_i >'^\tau, \tag{A.3}$$

$$V_{\text{Sym}} = \frac{V_{sym}}{2\rho_0} \sum_{i \neq j} (1 - 2|c_i - c_j|)\rho_{ij}, \tag{A.4}$$

$$V_{\text{Mom}} = \frac{1}{2\rho_0} \sum_{i \neq j} \left[\frac{V_{ex}^{(1)}}{1 + \left[\frac{\mathbf{P}_i - \mathbf{P}_j}{\mu_1 \hbar}\right]^2} + \frac{V_{ex}^{(2)}}{1 + \left[\frac{\mathbf{P}_i - \mathbf{P}_j}{\mu_2 \hbar}\right]^2} \right] \rho_{ij}, \tag{A.5}$$

$$V_{\text{Coulomb}} = \sum_{i \neq j} \frac{c_i c_j e^2}{2} \frac{1}{|\mathbf{R}_i - \mathbf{R}_j|} \text{erf}(\frac{|\mathbf{R}_i - \mathbf{R}_j|}{\sqrt{4\text{L}}}). \tag{A.6}$$

Here, erf denotes the error function, and c_i is 1 for protons and 0 for neutrons. We only take into account the effective interactions which affect nucleons. $< \rho_i >$ is an overlap of density with other nucleons in each event defined as

$$< \rho_i > \equiv \sum_{j(\neq i)} \rho_{ij} \equiv \sum_{j(\neq i)} \int d\mathbf{r} \rho_i(\mathbf{r}) \rho_j(\mathbf{r})$$

$$= \sum_{j(\neq i)} \frac{1}{(4\pi L)^{\frac{3}{2}}} e^{-\frac{(\mathbf{R}_i - \mathbf{R}_j)^2}{4L}}. \tag{A.7}$$

$< \rho_i >'$ means that L of $< \rho_i >$ is modified to be $L' = \frac{1}{2}(1 + \tau)^{\frac{1}{\tau}} L$. The parameters are listed in Table A.1. Calculated binding energy of nuclei by QMD with Metropolis sampling method under the condition $T = 2.5$ MeV is shown in Fig. A.1. Present effective interaction reproduces the global structure of the ground state property of the nuclei.

References

[1] G. F. Bertsch and S. Das Gupta, Phys. Rep. **160** (1988), 189, and references therein.

[2] W. G. Lynch, Ann. Rev. Nucl. Part. Sci. **37** (1987), 493.

[3] J. Pochadzalla et al. (ALADIN Collaboration), Phys. Rev. Lett. **75** (1995), 1040.
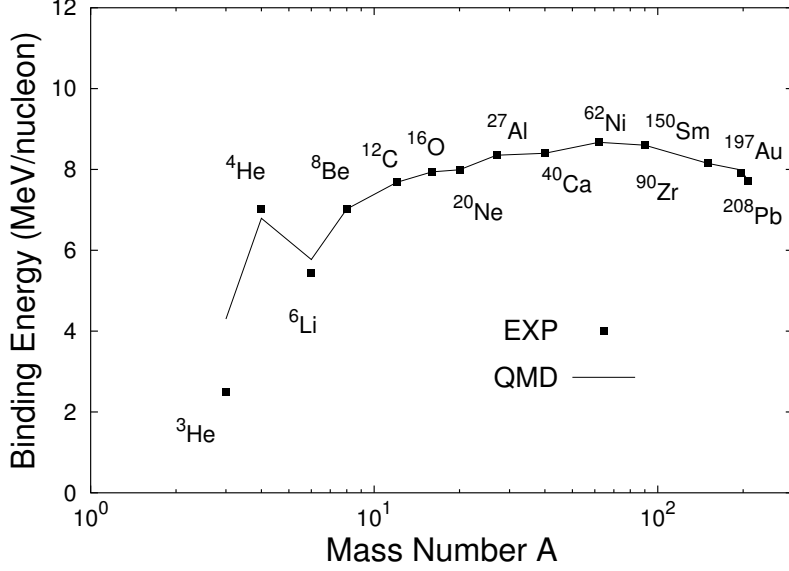
[4] M. D'Agostino et al., Phys. Lett. **B473**(2000), 219.

Fig. A.1. Calculated binding energy of nuclei by QMD with Metropolis sampling method under the condition $T = 2.5$ MeV.

Table A.1

QMD parameters

C_{Pauli}	140 [MeV]	V_{sym}	25.0 [MeV]
q_0	1.644 [fm]	$V_{ex}^{(1)}$	-258.54 [MeV]
p_0	120 [MeV/c]	μ_1	2.35 [fm^{-1}]
L	1.75 [fm^2]	$V_{ex}^{(2)}$	375.6 [MeV]
α	-127.86 [MeV]	μ_2	0.4 [fm^{-1}]
β	204.28 [MeV]	ρ_0	0.168 [fm^{-3}]
τ	$\frac{4}{3}$		

[5] W. Reisdorf et al. (FOPI Collaboration), Nucl. Phys. **A612** (1997), 493.

[6] R. Nebauer et al. (INDRA Collaboration), Nucl. Phys. **A658** (1999), 67.

[7] R. Nebauer and J. Aichelin, Nucl. Phys. **A681** (2001), 353c

[8] X. Campi, J. Phys. **A19** (1986), L917; X. Campi, Phys. Lett. **B208** (1988), 351; X. Campi, J. Phys. (Paris) **50** (1989), 183; X. Campi and H. Krivine, Nucl. Phys. **A589** (1995), 505.

[9] K.H. Tanaka et al (KEK-PS MULTI Collaboration), Nucl. Phys. **A583** (1995), 581.

[10] T. Murakami et al (KEK-PS/NIRS-HIMAC MULTI Collaboration), Proc. of the Int. Symp. on the Clustering Aspects of Quantum Many-Body Systems, Nov. 12-14, 2001, Kyoto, to appear; Private Communication (1999).

[11] Proposal for the 1998 GSIPAC; http://www-wnt.gsi.de/frs/toppage.html

[12] J. Cugnon, Nucl. Phys. **A462** (1987), 751;
J. Cugnon, C. Volant and S. Vuillier, Nucl. Phys. **A620** (1997), 475.

[13] A. V. Ignatyuk et al. Nucl. Phys. **A593** (1995), 519;
J. Benlliure, A. Grewe, M. de Jong, K. H. Schmidt and S. Zhdanov, Nucl. Phys.
A628 (1998), 458.

[14] W.-c. Hsi et al., Phys. Rev. **C60** (1999), 034609.

[15] A. E. Glassgold, W. Heckrotte and K. M. Watson, Ann. Phys. **6** (1959), 1.

[16] G. Wang, K. Kwiatkowski, V.E. Viola, W. Bauer, and P. Danielewicz, Phys.
Rev. **C53** (1996), 1811.

[17] T. Maruyama and K. Niita, Prog. Theor. Phys. **97** (1997), 579.

[18] W. Bauer, G.F. Bertsch, and H. Schulz, Phys. Rev. Lett. **69** (1992), 1888;
L. Phair, W. Bauer, and C.K. Gelbke, Phys. Lett. **B314** (1993), 271.

[19] Y. Nara, N. Otuka, A. Ohnishi, K. Niita, and S. Chiba, Phys. Rev. **C61** (2000),
024901.

[20] J. Aichelin, Phys. Rep. **202** (1991), 233.

[21] K. Niita, JAERI-Conf 96-009 (1996), 22.

[22] T. Maruyama, K. Niita, K. Oyamatsu, T. Maruyama, S. Chiba, and A.
Iwamoto, Phys. Rev. **C57** (1998), 655.

[23] T. Kido, T. Maruyama, K. Niita, and S. Chiba, Nucl. Phys. **A663&664** (2000),
877c.

[24] C. O. Dorso and J. Randrup, Phys. Lett. **B301** (1993), 328.

[25] A. Ohnishi and J. Randrup, Phys. Lett. **B394** (1997), 260.

[26] A. Ono and H. Horiuchi, Phys. Rev. **C53** (1996), 2958.

[27] T. Sjöstrand, Comput. Phys. Commun. **82** (1994), 74.

[28] H. Sorge, R. Mattiello, A. Jahns, H. Stöcker and W. Greiner, Phys. Lett. **B271**
(1991), 37; H. Sorge, L. Winckelmann, H. Stöcker and W. Greiner, Z. Phys.
C59 (1993), 85.

[29] L.A. Winckelmann, et al., Nucl. Phys. **A610** (1996), 116c; nucl-th/9610033;
S.A. Bass, et al., Prog. Part. Nucl. Phys. **41** (1998), 225; nucl-th/9803035.

[30] X. N. Wang, Phys. Rep. **280** (1997), 287.

[31] K. Werner, Z. Phys. **C42** (1989), 85; Phys. Rep. **232** (1993), 87.

[32] H. Sorge, H. Stöcker, and W. Greiner, Ann. Phys. **192** (1989), 266.

[33] K. Niita et al., Phys. Rev. **C52** (1995), 2620.

[34] H. Feldmeier, Nucl. Phys. **A515** (1990), 147;
H. Feldmeier, K. Bieler and J. Schnack, Nucl. Phys. **A586** (1995), 493.

[35] Y. Hirata, Y. Nara, A. Ohnishi, T. Harada, and J. Randrup, Prog. Theor. Phys.
102 (1999), 89.

[36] A. Ono and H. Horiuchi, Phys. Rev. **C53** (1996), 845.

[37] T. Maruyama, K. Niita, and A. Iwamoto, Phys. Rev. **C53** (1996), 297.

[38] M. Blann, Ann. Rev. Nucl. Sci. **25** (1975), 123.

[39] A. S. Botvina, A. S. Iljinov, and I. N. Mishustin Nucl. Phys. **A507** (1990), 649.

[40] W. Bauer, D. R. Dean, U. Mosel and U. Post, Phys. Lett. **150B** (1985), 53;
W. Bauer, U. Post, D. R. Dean, U. Mosel, Nucl. Phys. **A452** (1986), 699;
W. Bauer, Phys. Rev. **C38** (1988), 1297.

[41] W. Bauer, A. Botvina, Phys. Rev. **C52** (1995), R1760.

[42] M. K. Berkenbusch et al., nucl-th/0109062 (2001).

[43] S.B. Kaufman, M.W. Weisfield, E.P. Steinberg, B.D. Wilkins, and D.
Henderson, Phys. Rev. **C14** (1976), 1121.